ACCSCIENCE PUBLISHING

International Journal of Bioprinting

RESEARCH ARTICLE

Oozing: An accessible technique to create 3D-printed scaffolds suitable for tissue engineering

Juan Crespo-Santiago[1,2*], Luis M. Delgado[3], Rafa Madariaga[4], Laia Millan[1], Oriol Chico[1], Pau Oliver[1], Román Pérez[3], and Marta Otero-Viñas[2,5*]

[1]Elisava Barcelona School of Design and Engineering, University of Vic-Central University of Catalonia (UVIC-UCC), La Rambla 30, 08002, Barcelona, Spain

[2]Tissue Repair and Regeneration Laboratory (TR2Lab), Institute for Research and Innovation in Life and Health Sciences in Central Catalonia (IrisCC), Ctra. de Roda, 70 08500, Vic, Barcelona, Spain

[3]Bioengineering Institute of Technology, International University of Catalonia (UIC), Immaculada 22, 08017, Barcelona, Spain

[4]Data Analysis and Modeling Research Group (DAM), Department of Economics and Business, University of Vic-Central University of Catalonia (UVIC-UCC), Sagrada Família 7, 08500, Vic, Spain

[5]Faculty of Science, Technology, and Engineering. University of Vic – Central University of Catalonia (UVIC-UCC), C. de la Laura, 13, 08500, Vic, Barcelona, Spain

Abstract

Tissue-engineered constructs require mimicking the extracellular matrix microenvironment of native tissue for better promoting cell growth. Commercial three-dimensional (3D) printers provide a versatile platform to fabricate tissue models, but they possess certain constraints regarding the reproduction of natural tissue structures due to the limited functionality of current slicing strategies and hardware. In this study, we present a new approach to 3D-printing polylactic acid (PLA) constructs with fibers in the range of microns by combining the oozing effect and algorithm-aided design (AAD) with a conventional fused deposition modeling printer. Three different oozing geometries were compared with two controls to explore their mechanical behavior and their cellular culture growth potential. Microscopic analysis revealed that oozing groups possessed higher porosity and statistically significantly thinner fibers than controls. Sodium hydroxide treatment reversibly increased the hydrophilicity of PLA without affecting the scaffolds' mechanical properties in the compression tests. In addition, cell culture assays showed that oozing specimens exhibited a greater capacity of promoting SaOs-2 osteoblastic cell proliferation after 7 days in comparison with controls. We demonstrated that randomly distributed microfibered environments can be fabricated with an ordinary 3D printer utilizing the oozing effect and advanced AAD, resulting in improved biomimetic 3D constructs for tissue-engineering strategies.

Keywords: Oozing; 3D printing; Tissue engineering; Cell cultures; Polylactic acid

***Corresponding authors:**
Juan Crespo-Santiago
(jcrespo@elisava.net)

Marta Otero-Viñas
(marta.otero@uvic.cat)

Citation: Crespo-Santiago J, Delgado LM, Madariaga R, et al. Oozing: an accessible technique to create 3D-printed scaffolds suitable for tissue engineering. *Int J Bioprint*. 2024.
doi: 10.36922/ijb.2337

Received: November 29, 2023
Accepted: January 22, 2024
Published Online: March 12, 2024

1. Introduction

The demand for new tissues in regenerative medicine therapies has led to an increase in new tissue-engineering strategies to fabricate synthetic constructs for damaged

tissue replacement.[1,2] Tissue-engineered constructs or scaffolds require mimicking the microenvironment of the biological extracellular matrix (ECM) niche, composed of a microfibered complex that contributes to the mechanical support of the tissue.[3,4] The morphology and microstructure of scaffolds must satisfy specific mechanical and biological requirements including structure material organization, surface morphology, and proper porosity (pore size, distribution, and interconnectivity) to promote cell adhesion and proliferation, and subsequent ECM remodeling.[5,6]

Additive manufacturing technologies (three-dimensional [3D] printing) have become a promising approach to personalized regenerative treatments. These techniques are characterized by their design potential, high speed, and low cost, which allow the fabrication of tissue constructs from the micro- to the macro-scale, providing suitable structural and mechanical support for 3D cell cultures, thereby producing new, enhanced tissue.[7-12] Numerous types of constructs have been developed for several tissues using 3D printing for regenerative medicine: composites and polymers for bone tissue engineering,[13,14] cartilage for the meniscus,[15] or polylactic acid for vascular grafts,[16] among others.[17]

There are several sorts of additive manufacturing technologies that generate scaffolds for biomedical applications. Traditional modalities, such as fused deposition modeling (FDM), selective laser sintering (SLS), or stereolithography (SLA), among others,[18] allow the creation of components with micro-scaled geometries in various materials, such as polymers, composites, and metals with high accuracy and reproducibility.[19,20] Despite these advantages, many of these printing conditions are lethal to cells, such as high temperature or toxic chemicals. Hence, these techniques commonly generate acellular scaffolds that can be utilized for tissue-engineering purposes by seeding cells after fabrication.[21]

In contrast, recent techniques such as 3D bioprinting, in which a suspension of living cells together with suitable biomaterials and growing factors (bioink) is directly deposited to create 3D living tissue,[22] create interesting soft-tissue constructs, such as composites for ear regeneration,[23] or collagen for the human heart, in addition to many others.[24-26] 3D bioprinting can be classified according to American Society for Testing and Materials (ASTM) into: extrusion-based,[27] jetting-based,[28] and vat photopolymerization-based.[29] Although these techniques have a variety of applications, including trauma treatment, whole tissue creation, and *in vitro* drug testing, several drawbacks including bioink's dimensional stability, limited speed, or cell viability during printing process remain unsolved; therefore, soft materials like hydrogels are generally utilized for fabrication.[21,27,30]

FDM is one of the most widely utilized 3D printing technologies due to its versatility, simple maintenance, and low cost.[31,32] In comparison to others, this technique possesses many advantages, including availability of a wide range of biodegradable and biocompatible materials that can be printed, and compatibility with different CAD software. FDM has a simple working principle: A preformed polymeric thermoplastic filament is heated to a semiliquid state and then extruded through a nozzle directly onto the building platform following a programmed model, with thin layers being deposited on top of one another.[33-35] Moreover, no toxic solvents are needed to dissolve the polymeric filaments for printing, thus avoiding cell mortality when working with cell cultures.[36,37] Nevertheless, FDM has certain major constraints such as limited accuracy due to the thickness of the final extruded filament, the relationship between viscosity and nozzle diameter, or the high temperature applied during the melt-extrusion process that may change inherent material properties.[38]

Limited resolution is, particularly, one of the main disadvantages in FDM as the accurate impression is limited by the nozzle diameter.[39,40] Commonly, these nozzle diameters range from 0.8 mm to 0.2 mm, being unusual to find smaller diameters due to their easy clogging tendency and subsequent incapacity to ensure proper flow settings.[41,42] Furthermore, another well-known drawback of FDM printing occurs when the nozzle deposits a small amount of molten material and immediately moves to the next position. This movement creates the "stringing" effect or oozing: a very thin "hair" of molten material that extends across the direction of travel of the nozzle.[43,44] The oozing effect can be caused by a slow retraction speed, overheating in the extruder, high printing speed, or very long movements over open spaces, among others.[45-47]

The achievement of a microfiber-like environment represents a major feature to better mimic the tissue ECM niche. Several techniques such as electro direct writing,[48] electrospinning,[49,50] or melt-blowing[51] can create micro-scaled fibers, but FDM lacks the capacity to generate the thin required fibers due to the technique's own limitations. However, recent studies have successfully fabricated various arrays of microfibers leveraging the oozing effect, by the manipulation and implementation of certain parameters of the printing process, such as the printing speed or the feed rate, and combined them with algorithm-aided design (AAD).[44,52] Generally, these approaches can be found as a stack of parallel-like patterns with fibers in the range of hundreds of microns,[42] or as a combination of parallel-like

structures with layers of randomly distributed microfibers created by another technique (such as melt-spinning or electrospinning).[53,54] Although the fundamentals of this methodology have been similarly reported elsewhere,[44,52] AAD-controlled random distributions remain unexplored. These advances point to the direction of overcoming one of the fundamental architectural flaws of FDM, which is the macroscopic geometry of the fibers and subsequent macro-porosity of the scaffolds.

Several thermoplastic materials used in FDM printing include polylactic acid (PLA), acrylonitrile butadiene styrene (ABS), polycaprolactone (PCL), polyether ether ketone (PEEK), and nylon,[20,55] or other natural biopolymers.[56] PLA is a promising biopolymer in biomedical applications due to its properties such as biocompatibility, biodegradability, mechanical strength, process ability, and non-toxicity.[57] PLA scaffolds have been extensively utilized in bone tissue,[58] cartilage,[59] meniscus,[60] vascular tissue,[61] and other biomedical applications.[62] However, PLA has certain limitations concerning its use, such as a slow degradation rate and hydrophobicity, which affect cell adhesion to scaffold, rendering new tissue formation difficult.[61]

In this study, we developed algorithm-designed 3D constructs utilizing the oozing effect, employing both parallel and random distributions of the fibers (ranging from 30 μm up to a few hundred). In addition, we compared these constructs with ordinary FDM-printed scaffolds to analyze their cell growth potential. A selection of three different oozing-like geometries and two commonly manufactured controls were 3D-printed and fully characterized to better understand their architectural and mechanical properties together with their biological potential. The algorithm-controlled 3D random distribution of the microfibers in the oozing specimens in cell cultures represents a novel approach to developing a better biomimetic scaffold to be used in tissue-engineering repairing strategies.

2. Materials and methods

The research methodology employed to evaluate the scaffolds design and microstructure was based in 3 stages shown in Figure 1 and described in detail below in this section. A total of five experimental groups with five different infill geometries were selected for the study: Three groups were printed with oozing technique, and two controls were printed following standard procedure.

2.1. Design of the experimental infills

The three oozing specimens were designed following three different sequences: two of them with a parallel-fiber pattern, differentiated by a low-density knitting and a high-density knitting, respectively, and the third one with a random fiber pattern. In addition, two controls were designed with standard architectures: a waffle-like geometry and a gyroid (Figure 2). The five experimental groups, namely random oozing (Or), simple oozing (Os), complex oozing (Oc), gyroid (Gy), and waffle (Gof), were all designed cubic-shaped with an outer volume of 10 × 10 × 10 mm. All oozing groups, Os, Or, and Oc, were developed using the Silkworm (v0.0.1) plugin for Grasshopper3d

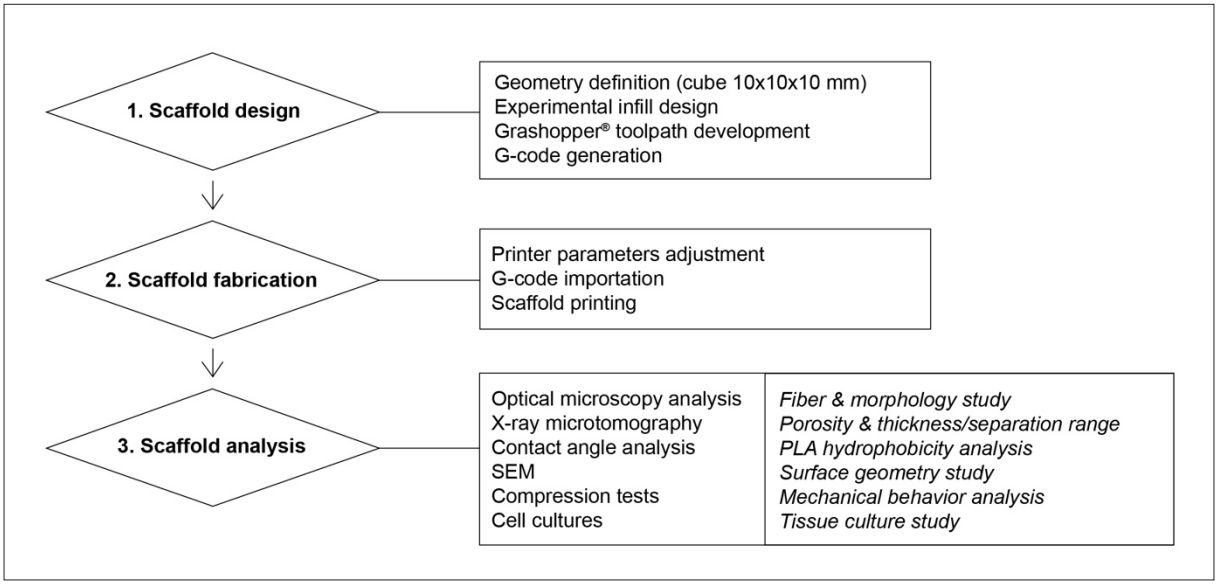

Figure 1. Stages of experimental methodology. Abbreviations: PLA, polylactic acid; SEM, scanning electron microscopy.

(Rhinoceros). Control group (Gof) was designed with CAD software, and Gy group was designed with Ultimaker Cura (v4.8.0, Ultimaker) slicer. All specimens were prepared for 3D printing with Ultimaker Cura (v4.8.0, Ultimaker) (**Figure S1** in Supplementary File).

The oozing print methodology was based on depositing a small drop of extruded material on a certain coordinate, then moving the nozzle to the next coordinate without extruding any material between both points. This method allows the generation of oozing fiber. The Or specimen was designed by distributing a random population of 60 points in each of the 4 lateral façades of a 10 × 10 × 10 mm cube, with a total of 240 points (Figure 2A1 and A2). The resulting lattice was created by assigning several random displacements of the nozzle on an *X*–*Y* plane, and then iterating different patterns at every layer of the *Z* axis. These displacements were generated and developed in Silkworm plugin by designing different tool paths (Figure 2C and D). The Os specimen was designed by creating a grid of 8 × 8 square spaces on a 10 × 10 mm *X*–*Y* plane (Figure 2B1 and B2). The *X*–*Y* planes were stacked along the *Z* axis, and each layer was rotated 90° from the previous one enabling the creation of the whole volume. The specimen was printed using the identical oozing methodology as with the Or specimen. Figure 2D shows the Grasshopper tool paths used for this specimen. The Oc specimen was designed following the same procedure as with the Os specimen by creating a grid of 12 × 12 square spaces on a 10 × 10 mm *X*–*Y* plane. Two commonly used infill patterns were selected as

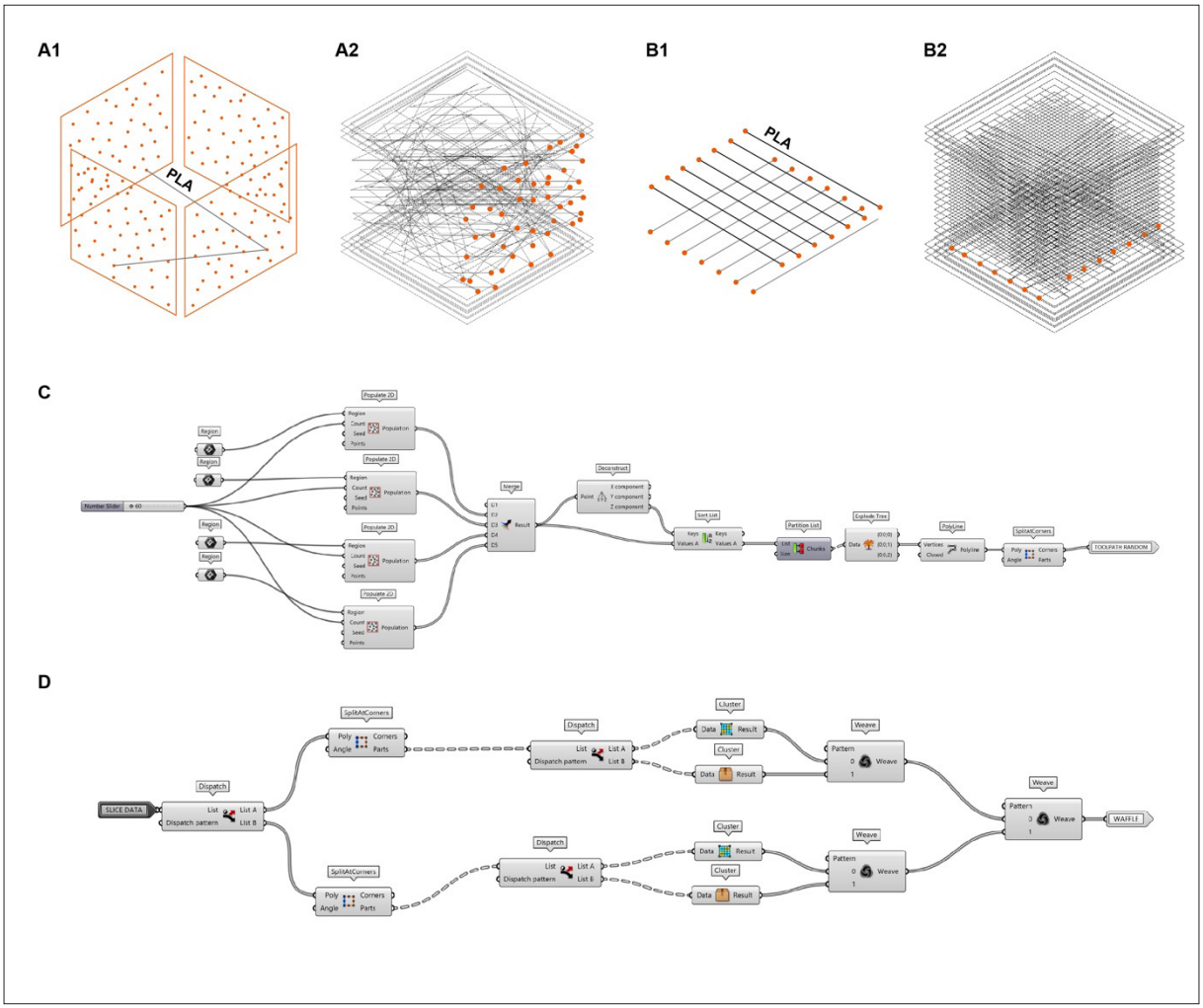

Figure 2. Schemes and toolpaths for scaffold design. Orange dots represent the nozzle stop, and black lines show the deposited material in form of oozing fibers. (A1) Planes showing the random distribution of 60 points created for Or specimen. (A2) Schematic of nozzle displacement path for Or specimen. (B1) Parallel pathways and planes created for Os specimen. (B2) Schematic of nozzle displacement path for Os specimen. (C) Grasshopper toolpath for Or specimen. (D) Grasshopper toolpath for Os specimen.

control groups: a gyroid geometry (Gy) and waffle-like geometry (Gof). The Gy specimen was generated using the gyroid infill form in Ultimaker Cura software creating four iterations in a 10 × 10 × 10 mm cube. The Gof sample was designed in SolidWorks (Dassault Systemes) as a 10 × 10 × 10 mm cube with an internal matrix of 5 × 5 equidistant holes of 1 × 1 mm.

2.2 Three-dimensional printing of scaffolds

All scaffolds were 3D-printed using an Ender-5 Pro printer (Creality 3D) equipped with a 0.4 mm nozzle and using 1.75 mm diameter PLA filament (Smartfil, Smartmaterials 3D), 210°C extrusion temperature, 60°C bed temperature, and 0.2 mm layer height. The printing speed was 80 mm/s for the control groups, with a feed rate of 1200 and constant flow rate. For the oozing groups, the printing speed was 59 mm/s, whereas the feed rate and the flow rate were set by Silkworm plugin (see Figure S2 for G-codes). For controls (Gy and Gof), G-codes were generated with Ultimaker Cura, with the .STL files imported beforehand. For experimental groups (Or, Os, and Oc), the G-codes were directly obtained and exported from Silkworm plugin (Grasshopper3d). After printing, all specimens were characterized, with the volume (x, y, and z) measured using a vernier caliper and the weight determined on a digital scale (Figure 3).

2.3. Porosity determination by X-ray microtomography

Porosity was measured using a Skyscan 1272 micro-CT (Bruker) at a 10 mm resolution. The X-ray source peak voltage was 50 kV with an intensity of 200 μA, 180° scanning, and a 0.2° step. The porosity was obtained using the CTAn software provided by Bruker. Ranges of thickness and separation distributions were also analyzed within this study (Figures 4 and 5).

2.4. Fiber thickness analysis

Fiber thickness was measured using a stereomicroscope (StereoBlue SB 1903, Euromex) with a digital camera (CMEX DC5000f, Euromex). Measurements were performed using the software ImageFocus Plus V2 (Euromex). For each experimental group, three samples were fabricated at five different heights (2 mm, 4 mm, 6 mm, 8 mm, and 10 mm) by directly stopping the 3D printer when the height of the sample reached the desired value. A total of three fibers were randomly selected at these five different heights per specimen. The thickness was measured at five points along each fiber: start (at the very beginning of the fiber), mid1 (an equidistant point from the middle and the start), center (at the middle point of the fiber), mid2 (an equidistant point from the middle and the end), and end (a point very close to the end of the fiber). However, regarding Gy and

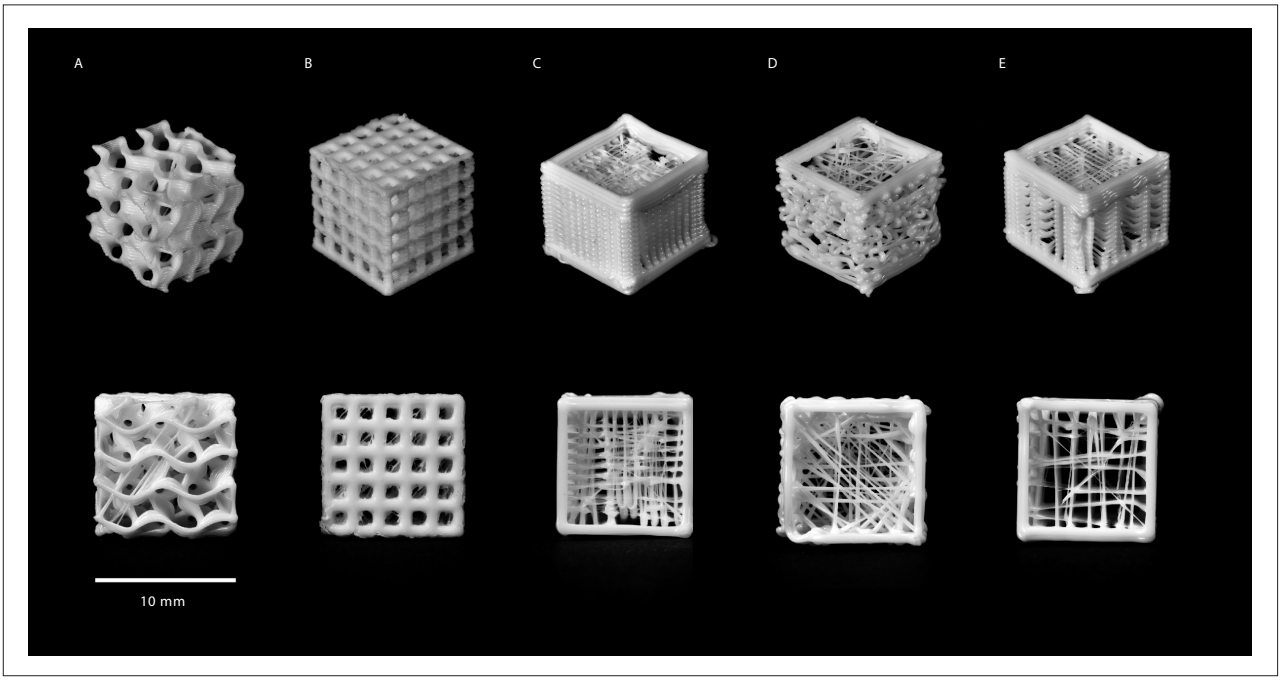

Figure 3. 3D-printed PLA experimental groups with different knitting patterns. (A) Gy: gyroid architecture; (B) Gof: waffle-like architecture; (C) Oc: oozing with parallel dense knitting; (D) Or: oozing with random knitting; and (E) Os: oozing with parallel low-dense knitting. Images in the top row present perspective view of the specimens, and the bottom row shows top-view images of the specimens.

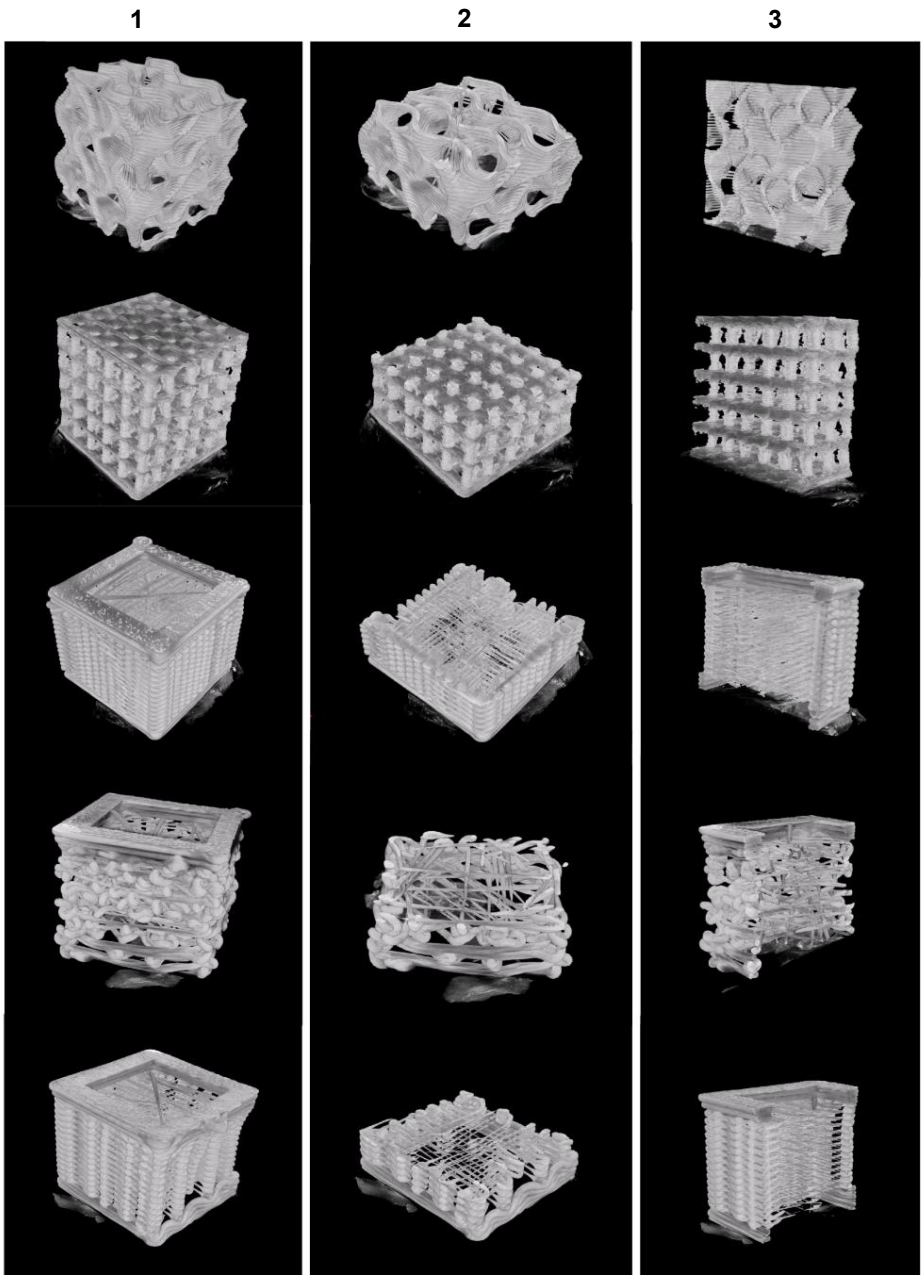

F

Specimen	Volume (mm^3)	SD	Mass (g)	SD	Porosity (%)
Or	1213	11.97	0.319	0.011	83.66
Oc	1188	27.09	0.413	0.010	77.78
Os	1200	25.47	0.327	0.003	86.58
Gy	1071	20.69	0.329	0.007	76.04
Gof	1227	22.38	0.486	0.017	67.83

Figure 4. X-ray microtomography reconstructions of the five specimens. (A) Gy, (B) Gof, (C) Oc, (D) Or, and (E) Os. Column 1 shows perspective views of the specimens, column 2 shows the top views, and column 3 shows the lateral views of the specimens. (F) Physical characteristics (volumes, masses, and total porosity) of the specimens (n = 10).

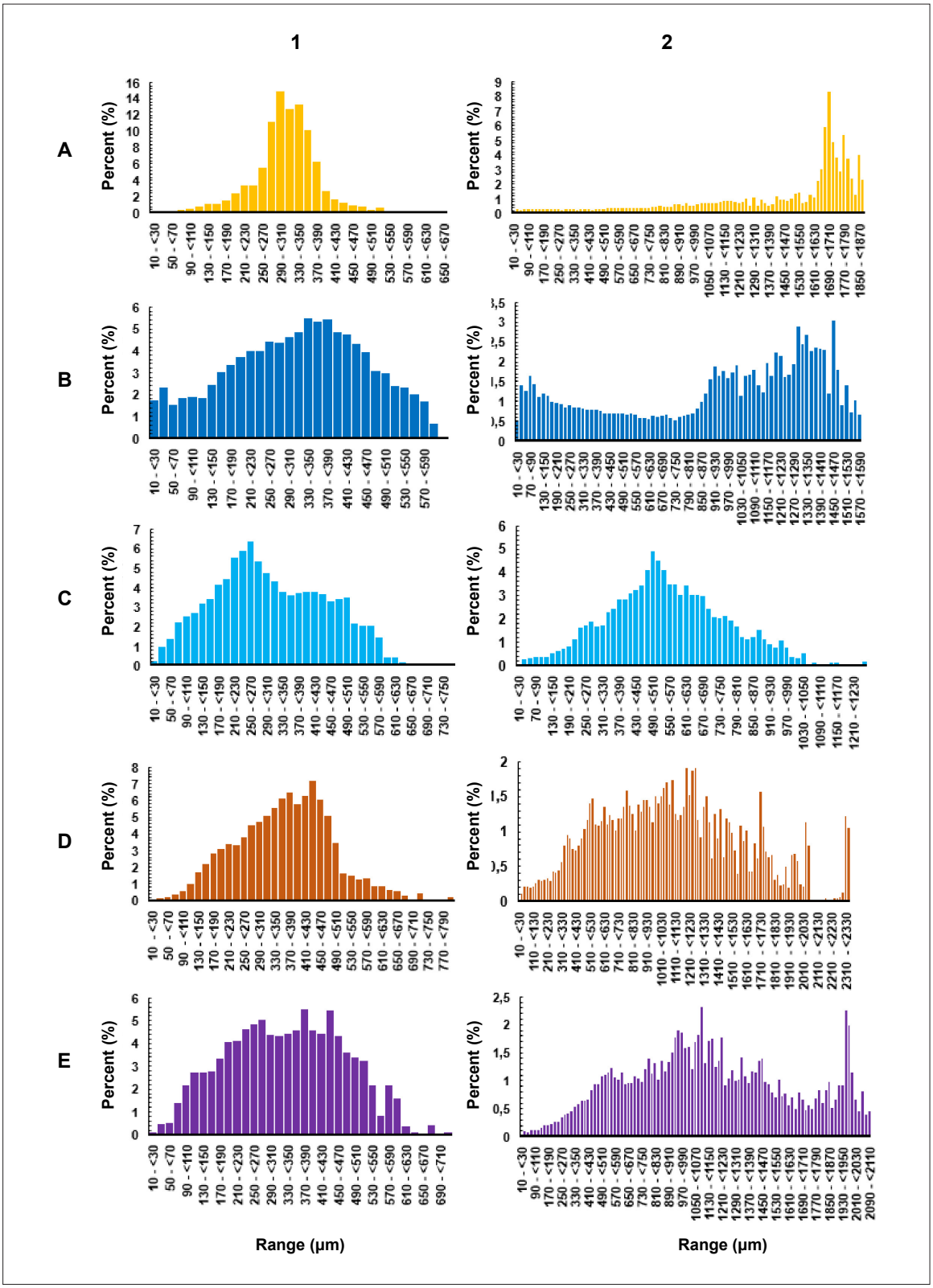

Figure 5. Range distributions for (A) Gy, (B) Gof, (C) Oc, (D) Or, and (E) Os. Column 1 shows thickness distribution, and column 2 shows fiber separation distribution.

Gof, geometries we measured the grid thickness instead of shred thickness, as they do not possess proper fibers as the oozing groups (Figure 6).

2.5. Effect of sodium hydroxide treatment

Scaffolds were submerged in a sodium hydroxide solution (NaOH, 2 M solution, Sigma-Aldrich) for 15 min at room temperature. Then, the samples were washed for 5 min in distilled water three times.

2.6. Scaffold surface analysis

The specimens were coated with a gold layer using an agar sputter coater (AGB 7340, AgarScientific) and analyzed with a scanning electron microscope (SEM, JSM 5410, JEOL) operated at 10 kV. A total of four regions per scaffold were studied (Figure 7).

2.7. Contact angle assays

Water contact angle was assessed using PLA discs with a contact angle measuring system (OCA 15, Dataphysics) using the sessile drop method. For these assays, six PLA discs (10 mm in diameter and 2 mm in height) were 3D-printed using the same parameters described above with a 100% infill. A distilled water drop (3 µL) was generated at 1 µL/s, and photographs were captured for posterior analysis using SCA 20 software (Dataphysics) (Figure 8).

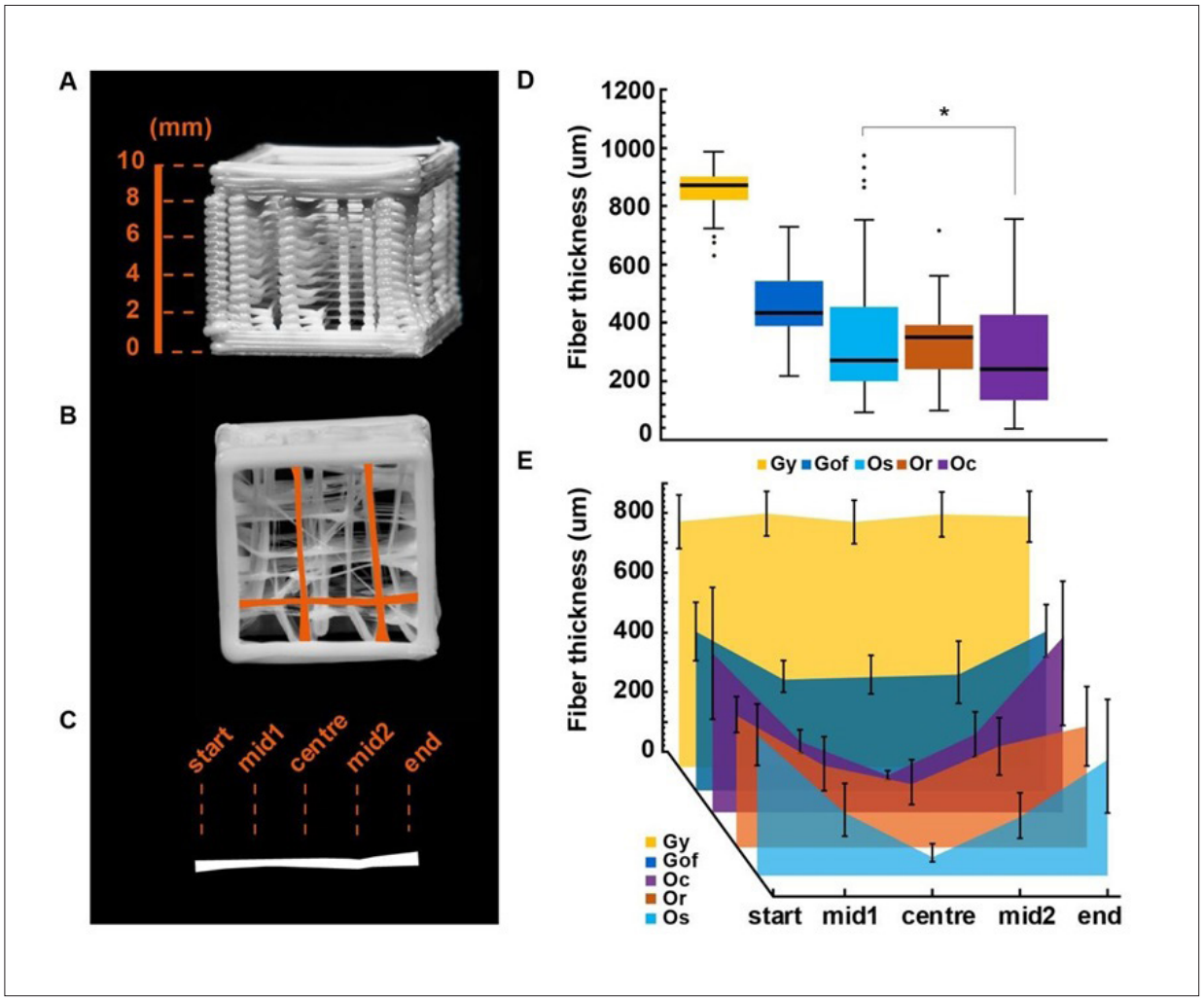

Figure 6. Fiber thickness analysis. (A–C) Scheme of the fiber thickness measuring setup. (A) Scheme of the five different heights (2, 4, 6, 8, and 10 mm) for performing fiber measurements. (B) Example of three randomly selected fibers at each height of the sample to perform the fiber thickness analysis. (C) Representation of five selected points to measure thickness along the fiber (start, mid1, center, and end). (D) Fiber thickness means measurements per specimen ($n = 45$, * $p < 0.05$ by Kruskal–Wallis test). (E) Thickness measurements across the fiber per specimen.

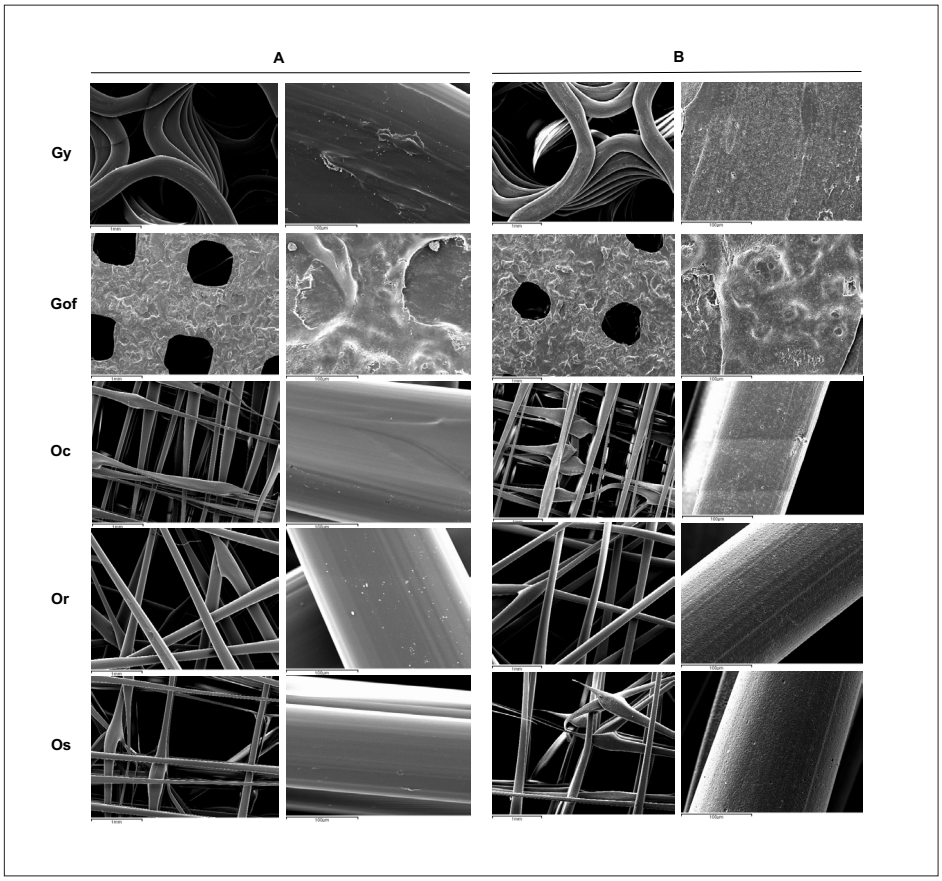

Figure 7. Specimens surface analysis by scanning electron microscopy. (A) Control specimens' images (prior to treatment) and (B) specimens images after NaOH treatment. Scale bar: 100 μm.

2.8. Compression tests

A total of five specimens per condition (control and treated with NaOH) for each experimental group were tested on a universal testing machine (Z005, Zwick) equipped with a 2.5 kN load cell and compression plates. The load and displacement values of the tested specimens were recorded, and the compression stress and strain were calculated according to the obtained load and displacement after the experiments. The loading rate was at 5 mm/min (Figure 9). E modulus was calculated at the linear elastic deformation region using a linear regression included in TestXpert II (Zwick).

2.9. Cell cultures

SaOs-2 cell line (Sigma-Aldrich) was cultured in McCoy's 5A medium (Fisher Scientific), supplemented with 10% fetal bovine serum (FBS, Sigma) and 1% penicillin–streptomycin (Fisher Scientific). A total of 300,000 cells were seeded per scaffold. Cells were incubated for 1, 3, and 7 days at 37°C, under a condition of 5% CO_2 and 95% humidified air. Metabolic activity was assessed by performing a resazurin reduction assay. Briefly, seeded cells were incubated with cell culture medium (600 μL) containing resazurin (10 μg/mL) sodium salt (Sigma) for 2 h at 37°C, under a condition of 5% CO_2 and 95% humidified air. Then, 100 μL of cell culture medium were transferred to a 96-well plate, and absorbance was measured at 570 nm and 600 nm using a microplate reader (Synergy HT Multi-detection Microplate Reader, Bio-Tek). Cell metabolic activity was expressed in terms of percentage reduction of resazurin and normalized to control values obtained from tissue culture plastic (TCP) of the same day.

Immunological assays to observe cell adhesion to the scaffolds were performed and observed using a confocal microscope (CLSM, TCS SP8, Leica Microsystems). Briefly, after 7 days of seeding, scaffolds were washed with phosphate-buffered saline (PBS) to remove dead cells. Then, the scaffolds were fixed using 4% paraformaldehyde (PFA) for 30 min and washed with PBS three times. Acti-Stain 488 phalloidin antibody (Cytoskeleton, Inc.) was used for cytoskeleton staining by diluting it in PBS (7 μL per mL), and scaffolds were

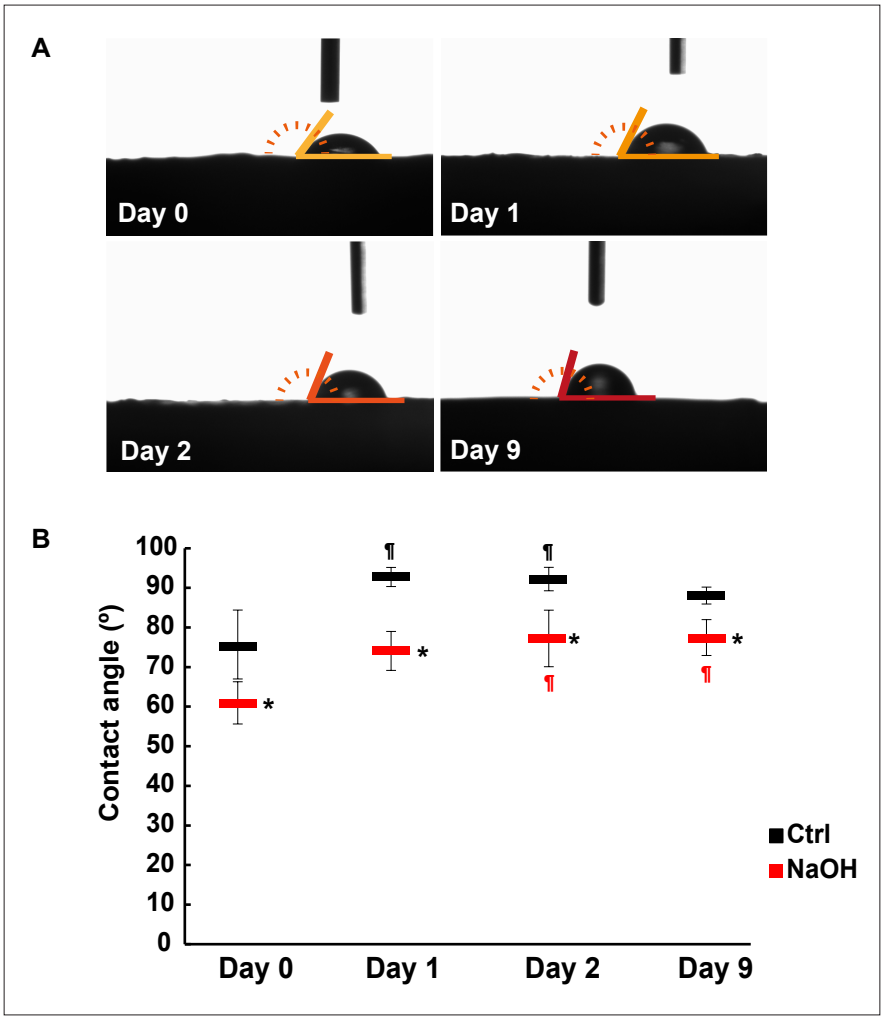

Figure 8. Water drop contact angle assays. (A) Scheme of water drop contact angle determination at different tested times. (B) Contact angle measurements at day 0, day 1, day 2, and day 9 in control groups and NaOH-treated groups. ($n = 6$, * and ¶ $p < 0.05$ by Kruskal–Wallis test)

incubated for 45 min with the solution (500 µL). Then, scaffolds were washed three times with PBS. Cell nuclei were stained using DAPI ready-made solution (Sigma-Aldrich) diluted at 1:1000 in PBS and incubated for 30 s. Finally, the scaffolds were washed with PBS and were observed in the confocal microscope using the Alexa 488 and DAPI filters and z-stacking. All assays were performed in triplicate (Figure 10).

2.10 Statistical analysis

All results are expressed as means ± standard deviation (SD). All data were analyzed using different tests of equality of means, with a confidence level of 95% ($p < 0.05$). First, Kolmogorov–Smirnov test was deployed to assess data normality. The results of normality tests dictate the different methods used for testing: in cases where the data were normally distributed, an analysis of variance (ANOVA) test was used to compare means of samples, or else, Kruskal–Wallis tests were used.

3. Results

3.1. Observations of the scaffolds

The five experimental groups—Gy, Gof, Oc, Or, and Os—are presented in Figure 3, captured in perspective (top) and top views (bottom), respectively. The unique features of each scaffold were clearly displayed, and the different knitting patterns could be observed. Figure 3A shows the gyroid geometry (Gy), and Figure 3B shows the waffle-like geometry of (Gof). Figure 3C and E show the predominant parallel pattern created using the oozing technique, in a dense grid (Oc) and in a lesser dense grid (Os), respectively. Figure 3D shows the aleatory pattern of Or, where fibers do not follow any predominant direction. A very important

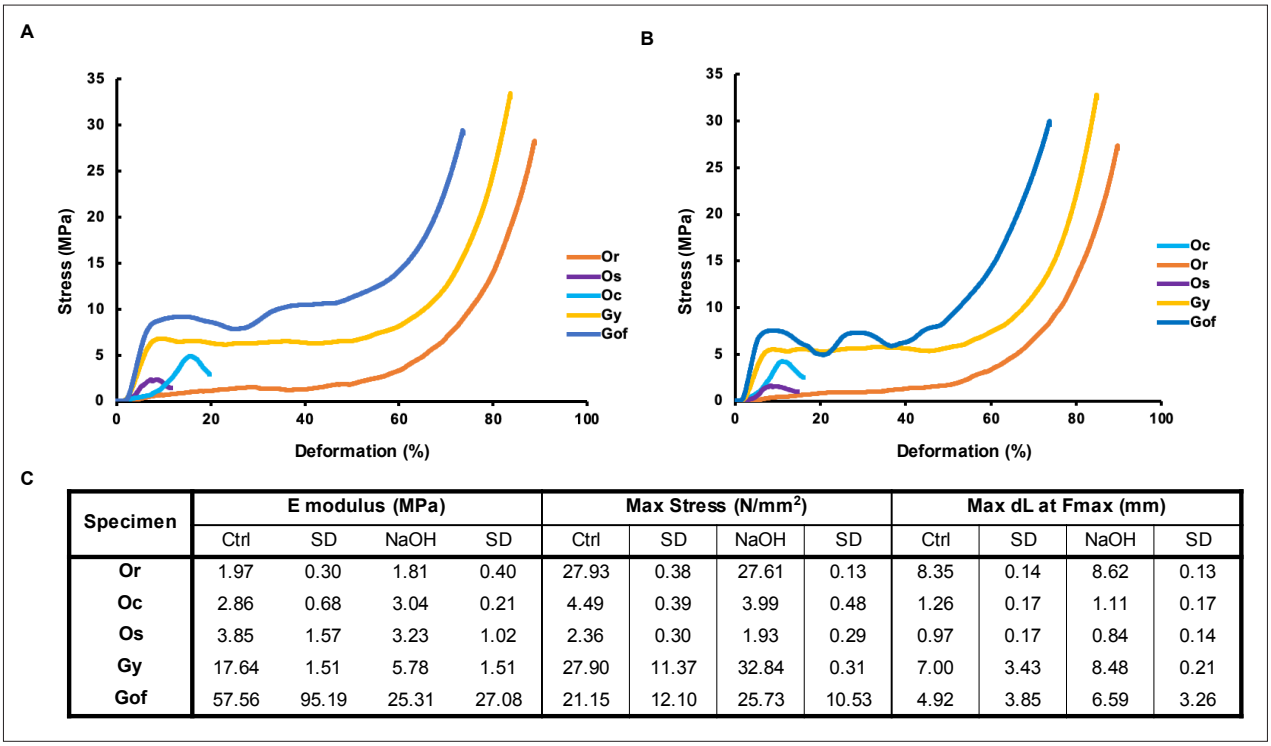

Specimen	E modulus (MPa)				Max Stress (N/mm²)				Max dL at Fmax (mm)			
	Ctrl	SD	NaOH	SD	Ctrl	SD	NaOH	SD	Ctrl	SD	NaOH	SD
Or	1.97	0.30	1.81	0.40	27.93	0.38	27.61	0.13	8.35	0.14	8.62	0.13
Oc	2.86	0.68	3.04	0.21	4.49	0.39	3.99	0.48	1.26	0.17	1.11	0.17
Os	3.85	1.57	3.23	1.02	2.36	0.30	1.93	0.29	0.97	0.17	0.84	0.14
Gy	17.64	1.51	5.78	1.51	27.90	11.37	32.84	0.31	7.00	3.43	8.48	0.21
Gof	57.56	95.19	25.31	27.08	21.15	12.10	25.73	10.53	4.92	3.85	6.59	3.26

Figure 9. Stress–strain curve for compression tests. (A) Representative curves for compression assay in control samples (prior to treatment). (B) Representative curves for compression assays in samples after NaOH treatment. (C) Results for E modulus, maximum stress, and maximum elongation at maximum stress per each specimen group ($n = 5$ per experimental group and per condition, $p < 0.05$).

fact that we observed in the oozing groups is that fibers never touch each other in the interior knitting.

3.2. Volume and mass measurements

The outer volumes determination showed similar values between Gy and Oc, and both have statistical differences ($p < 0.05$) with Or, Os, and Gof (Figure 4F). In the case of Gy, this difference may be attributed to the design of the geometry of Gy itself, as this specimen does not possess a supporting frame like the others. This lack of structural support for the (Gy) specimen may have led to a certain shrinkage of the structure after printing (**Figure S1** in Supplementary File). Masses were found to differ between specimens, with Gof being the heaviest of them all, followed by Oc, then Gy and Os with similar weights, and Or was the lightest (Figure 3F). Our results demonstrated that the density of the inner knitting pattern varies considerably from one specimen to another and therefore the amount of extruded material in each specimen.

3.3. X-Ray microtomography porosity

The X-ray scanning and reconstruction analysis of all the specimens' geometry allowed the appreciation of the actual inner geometry of the scaffolds and performing their physical characterization (Figure 4A–E). The mass and total porosity analysis of the specimens demonstrated a direct correlation with the amount of extruded material, with the oozing specimens—Oc, Or, and Os—being the most porous and, hence, the lightest ones, in contrast with control groups (Gy and Gof). The thickness distribution determination showed a very similar profile in all oozing groups (Oc, Or, and Os) and in control groups (Gof and Gy), with the majority ranging from ~30 μm to ~630 μm (Figure 5). However, the thickness distribution was much more concentrated in the range of ~310 μm to ~390 μm in Gy specimen. In terms of the separation distribution, our results showed many similarities between groups, but with different pattern distributions: a marked skew right pattern for Gy specimen, a tendency to a uniform distribution in Gof, Oc, and Or displaying a symmetric unimodal pattern, and a multimodal distribution in Os group. In addition, Gof, Or, and Os showed a more scattered separation pattern. The biggest separation distribution and the most concentrated were found in Gy group, as the values range from 1630 μm to 1830 μm. In contrast, the smallest separations were found in Oc group, as it possessed the densest knitting pattern.

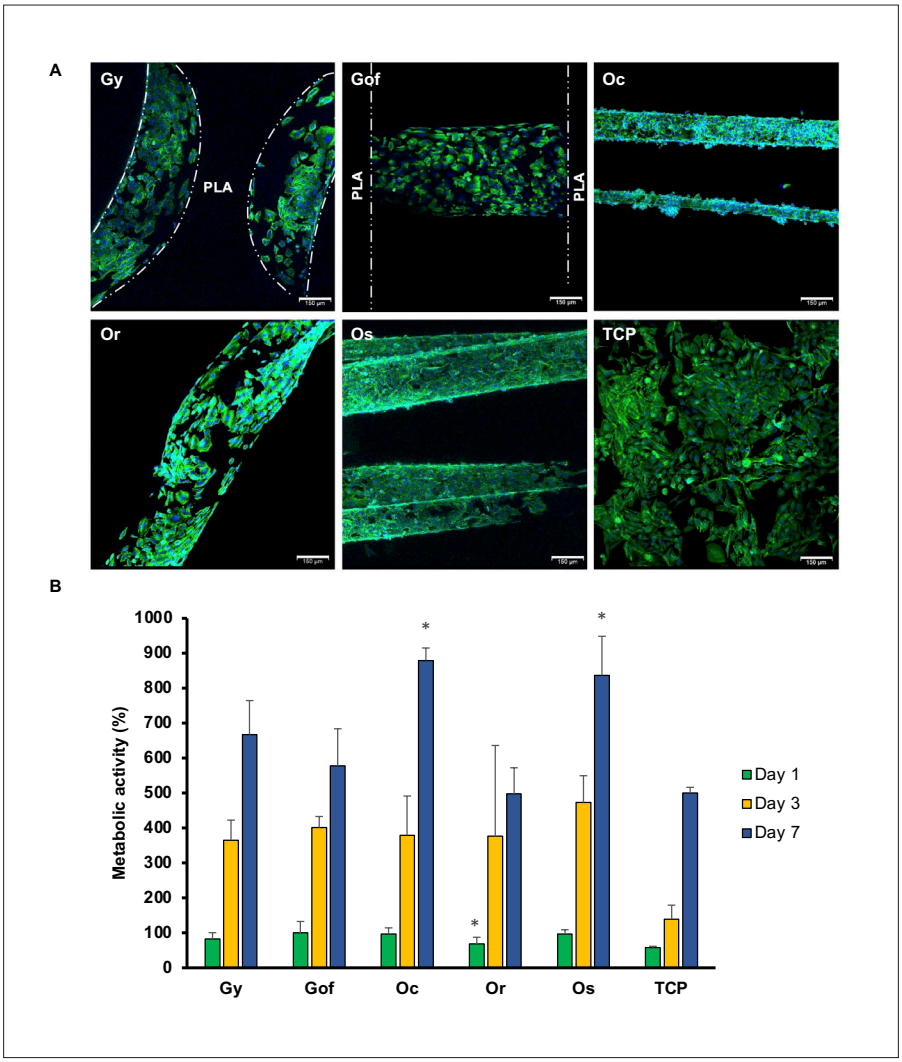

Figure 10. Cell culture assays in the scaffolds. (A) Representative immunofluorescence images of confocal microscopy of cell culture onto the different scaffolds (Gy, Gof, Oc, Or, and Os) and in control (TCP) at day 7 after seeding. Nuclei were stained with DAPI and cytoskeleton with phalloidin. Scale bar: 150 µm. (B) Metabolic activity at days 1, 3, and 7 ($n = 3$, $p < 0.05$ Mann–Whitney test).

3.4. Fiber thickness

The results of fiber thickness measurements at five different selected points in each fiber (Figure 6A–C) demonstrated statistically significant differences ($p < 0.05$) between the oozing groups (Or, Oc, and Os) and the control groups (Gy and Gof), with the fibers in the oozing group relevantly thinner than in the controls (Figure 6D).

All oozing specimens showed greater thickness at the end of the fibers and a progressive narrowing as it reached the center of the fiber. This characteristic was common to all samples. Specimen Gof showed more constant values, and specimen Gy displayed almost equal values in every measured point. Although the mean values of fiber thickness were found to be similar at the beginning (start) and at the end (end) of the fibers, measurements in the center of the fiber (center) varied depending on the specimen, and were narrower in the oozing groups (Os, Oc, and Or), ranging from ~70 µm to ~240 µm, than in the (Gof) or (Gy) groups, which displayed less difference in thickness. These results may be related to the fact that the control groups were not properly fabricated with oozing techniques but with regular FDM nozzle deposition (Figure 6E).

3.5. NaOH treatment

With scanning electron microscopy (SEM) analysis, we studied several images of regions of interest (ROI) on the surface of the scaffolds to compare the surface aspect prior to and after NaOH treatment (Figure 7A–B). Our results

demonstrated that NaOH solution erodes the surface of the fibers. In addition, the hydrophilicity assay showed statistically significant differences (* $p < 0.05$) between controls and NaOH-treated groups at each measuring point (day 0, day 1, day 2, and day 9), with a constant shift of ~9° to 15° observed between conditions. Similarly, statistically significant differences in contact angle within time were separately found in both conditions. Additionally, the contact angle in the controls was statistically significant ($'p < 0.05$) between day 0 and day 1, and between day 0 and day 2. However, the NaOH-treated group showed differences between day 0 and day 2, and between day 0 and day 9 (Figure 8).

3.6 Compression study

Our results from the determination of elastic modulus (E), maximum stress (Max stress), and maximum elongation at maximum force (Max dL at F_{max}) for all scaffolds in both experimental conditions (NaOH treatment and control) demonstrated no statistically significant differences ($p < 0.05$) between conditions for any studied parameter, indicating that treatment does not affect mechanical properties (Figure 9). Interestingly, Gy and Gof specimens' data showed a higher E modulus in both conditions (NaOH treatment and control) compared to the oozing groups, with Gof's being three or four times higher than that of Gy. Maximum stress values showed similar behavior in both experimental conditions for all specimens, except for Oc and Os, which were found to be considerably lower. Maximum elongation at maximum force showed similar results in both conditions for all specimens with a lower value in Oc and Os specimens (Figure 9C).

3.7. Cell culture studies

To assess how the morphology or accuracy of the 3D-printed structure could affect the cell response, SaOs-2 cells were seeded and cultured within the scaffolds. Metabolic activity was determined using a resazurin salt reduction assay, and cytoskeleton staining was observed with a confocal microscope (Figure 10A). Tissue culture plastic (TCP) was used as a control for cell behavior while Gof, commonly used in tissue-engineering applications, was used as a control of the infill structure. As shown in Figure 10B, there was no difference in the initial adhesion (day 1) of cells to the different scaffolds, except for Or, which displayed a significantly lower cell adhesion ($p < 0.05$). However, this lower metabolic activity was not statistically significant at days 3 and 7. Moreover, the metabolic activity was gradually increased during the culture time, being comparable to that of Gof and normal TCP, and was significantly higher for Os and Oc at day 7 ($p < 0.05$). These results correlated with higher density of fibers per volume in the Os and Oc scaffolds. The immunofluorescence results (Figure 10B) were consistent with the metabolic activity, showing that scaffold walls of Gy and Gof were mostly covered by spread cells at day 7. Similarly, fibers of Os, Or, and Oc were also completely covered by spread cells.

4. Discussion

Oozing or stringing effect has been generally described as a non-desirable drawback in FDM.[38,62] Despite these considerations, some recent studies have developed interesting approaches utilizing this effect to design environments with fibers in the range of microns (from a few tens up to hundreds). Various geometries have been studied by means of this technique, such as planar parallel arrangements,[44,63] 3D parallel distributions,[51,59,64] and also hybrid constructions, combining FDM with another technique, such as airbrushing[54] or electrospinning,[65] in order to create a stack of alternate layers. Nevertheless, these approaches still fail to produce an improved biomimetic 3D environment with randomly distributed fibers, as they all remain gridded.[66-68]

Our study focused on developing a set of novel FDM-printed constructs with random and gridded distributions of microfibers that may better mimic those of the native ECM niche. In addition, we analyzed the potential of these constructs, which support cell culture growth, as bone tissue-engineering strategies. This may represent an important progress, as we introduced for the first time the potential of using the oozing or stringing phenomenon to enhance the 3D-printed scaffolds characteristics for better promoting cell attachment and growth, as the created fiber dimensions better matched the ECM natural niche.[69,70]

We demonstrated that design is a fundamental tool to overcome FDM printing limitations when using conventional printing machines. Our results showed that it is possible to surpass the constraints of an accessible FDM ordinary printer by using AAD to improve the architecture of the scaffolds, corroborating similar algorithm-based methodology previously described in the literature.[65] Moreover, our scaffolds' design algorithms were especially designed to create random distributions of the fibers, providing an innovative framework that enhances the FDM printing application to an improved biomimetic-like approach in the tissue-engineering field.[70-72]

Our results demonstrated the oozing effect is a repeatable technique that can be controlled considering a certain degree of tolerance within fiber geometry. An accurate setting of the printing parameters, such as feeding speed and printing speed, among others, and other intrinsic

variables like temperature and relative humidity of the ambience have been reported to reduce fiber geometrical variability.[44] Despite these considerations, a certain degree of heterogeneity can be expected when working with the oozing technique.[51]

Our results showed that the scaffolds of the oozing groups exhibited an enhanced cell attachment and proliferation within 7 days of culture in comparison with controls. These results are possibly attributed to the microscale of the fibers together with an increased porosity of the whole construct, as suggested elsewhere.[42,73] These data increase the knowledge about the utility of FDM oozing-created constructs as scaffolds for growing cells, in concordance with other previous publications. Nevertheless, further culture assays should be performed to confirm and improve the understanding of their biological potential as a tissue-engineering strategy.[57]

Regarding fiber geometry, we found that oozing groups possessed dispersed fiber thickness depending on the point they were measured, with the lowest measurement found in the middle of the fiber in every case, in agreement with other studies.[73] In contrast, controls (Gy and Gof) presented notably more homogeneous fiber thickness, due to the fact that their infill cannot be considered a proper fiber but a regular FDM deposition.[5,54] Oozing groups exhibited statistically significant thinner fibers than controls, corroborating that the oozing effect can achieve considerably narrower fibers than standard FDM printing as it has been proven in the literature.[44,51] Acquiring a better control over the range of thicknesses for every printed fiber with the oozing technique would represent a major advance for creating tissues with different fiber arrangements. Printing speed together with flow rate and feed rate are fundamental variables to be mastered in future works as pointed elsewhere.[41,45,73]

As observed, a scaffold's porosity grade was directly related to mechanical behavior as an increase in the inner voids led to a lower compressive strength. These results are in agreement with other reported publications, which described the scaffold porosity being inversely proportional to mechanical strength, resulting in a less dense construct that can only withstand lower stress.[56,74] Interestingly, it has been described that mechanical strength is geometry-dependent. Fernandez-Vicente et al.[35] described a series of constructs with different infill patterns and the same mass that showed different mechanical behavior as certain specimens supported greater mechanical loading depending on their pattern design. Despite these observations, the influence of the geometry pattern caused a variation of less than 5%.

Polylactic acid is a well-known biocompatible polymer extensively used in biomedical applications. However, it has certain limitations concerning its use such as a slow degradation rate and strong hydrophobicity that can interfere with cell adhesion.[56,60] Alternatively, our results demonstrated that the NaOH treatment can increase the hydrophilicity characteristics of the PLA scaffold and maintain them nearly 9 days, enhancing the potential of PLA in bioengineering tissue applications. Furthermore, our data demonstrated that control specimens showed a similar behavior to NaOH-treated specimens, suggesting that FDM printing itself (melting and extruding process) modifies PLA's hydrophilic superficial properties. This temporally increased hydrophilicity proposes a certain reversibility of the process when PLA is 3D-printed, corroborating other published studies.[75] Interestingly, NaOH treatment of the constructs did not affect their mechanical behavior, probably due to the treatment only affecting the surface of the scaffolds, as previously described.[57]

With good cell adhesion and proliferation activity on the scaffolds in all tested specimens, our data support the application of this new set of scaffolds in tissue engineering. In addition, in the cases of Oc and Os specimens, the cell activity observed was higher than in the other specimens. These results may be justified by the smaller fiber separation in these two specimens in comparison with Or and controls (Gof and Gy) that could allow increased cell density in the scaffold pores. This cell density could promote greater cellular proliferation and occupancy in these constructs, as it has been noted in other reports.[67,76] Nevertheless, these results may be confirmed with ulterior studies in the field.

5. Conclusion

The oozing technique together with our AAD-controlled random distribution provides an interesting platform to create 3D-printed scaffolds with fibers in the range of microns that may better mimic the ECM niche than those fabricated by conventional FDM without advanced programming. The benefits of this technical approach are reliant on its capacity to overcome the limitation of the extruded filament's diameter, and the typical parallel-like distribution of the scaffolds. Nonetheless, we are cognizant of the necessity to better control the oozing process to improve the mastering of the thickness and geometry of fibers. Our strategy to combine AAD with an accessible 3D printer together with cell culture assays represents a powerful approach to creating novel biomimetic constructs with great potential suitable for tissue engineering.

Acknowledgments

None.

Funding

The authors would like to thank the Government of Catalonia [2017 SGR 708 and 2021 XARDI 00002]; the Spanish Ministry of Science and Innovation Ramón y Cajal fellowship [RYC2018-025977-I]; MINECO/FEDER Project [RTI2018-096088-J-100]; and the PO FEDER of Catalonia 2014ᴄ32020 [project PECT Osona Transformació Social, Ref. 001-P-000382].

Conflict of interest

The authors declare no conflicts of interest.

Author contributions

Conceptualization: Juan Crespo-Santiago
Data curation: Laia Millan, Oriol Chico, Pau Oliver
Formal analysis: Juan Crespo-Santiago, Rafa Madariaga
Funding acquisition: Marta Otero-Viñas, Roman Perez
Investigation: Juan Crespo-Santiago, Luis M. Delgado, Laia Millan, Oriol Chico, Pau Oliver
Methodology: Juan Crespo-Santiago
Resources: Luis M. Delgado
Validation: Juan Crespo-Santiago
Visualization: Juan Crespo-Santiago
Writing – original draft: Juan Crespo-Santiago
Writing – review & editing: Marta Otero-Viñas, Luis M Delgado

Ethics approval and consent to participate

Not applicable.

Consent for publication

Not applicable.

Availability of data

G-codes can be downloaded directly from: https://github.com/JuanCrespoSantiago/Oozing-Gcodes.git

References

1. Langer R, Vacanti JP. Tissue engineering. *Science*. 1993;260(5110):920-926. doi: 10.1126/science.8493529
2. Ikada Y. Challenges in tissue engineering. *J R Soc Interface*. 2006;3(10):589-601. doi: 10.1098/rsif.2006.0124
3. Shin H, Jo S, Mikos AG. Biomimetic materials for tissue engineering. *Biomaterials*. 2003;24(24):4353-4364. doi: 10.1016/S0142-9612(03)00339-9
4. Yue B. Biology of the extracellular matrix: an overview. *J Glaucoma*. 2014;23(8):S20-S23. doi: 10.1097/IJG.0000000000000108
5. Ceretti E, Ginestra P, Neto PI, Fiorentino A, da Silva JVL. Multi-layered scaffolds production via fused deposition modeling (FDM) using an open source 3D printer: process parameters optimization for dimensional accuracy and design reproducibility. *Procedia CIRP*. 2017;65:13-18. doi: 10.1016/j.procir.2017.04.042
6. Jiang X, Zheng W, Takayama S, Chapman RG, Kane RS, Whitesides GM. Micro-scale patterning of cells and their environment. In: Lanza R, Langer R, Vacanti JP, eds. *Principles of Tissue Engineering*. 4th ed. Cambridge, Massachusetts: Elsevier Inc.; 2013: 359-384. doi: 10.1016/B978-0-12-398358-9.00019-7
7. Richards DJ, Tan Y, Jia J, Yao H, Mei Y. 3D printing for tissue engineering. *ISR J Chem*. 2013;53(9-10):805-814. doi: 10.1002/ijch.201300086
8. Lee M, Wu BM. Recent advances in 3D printing of tissue engineering scaffolds. *Methods Mol Biol*. 2012;868:257-267. doi: 10.1007/978-1-61779-764-4_15
9. Choi JW, Kim N. Clinical application of three-dimensional printing technology in craniofacial plastic surgery. *Arch Plast Surg*. 2015;42(3):267-277. doi: 10.5999/aps.2015.42.3.267
10. Jakus AE, Secor EB, Rutz AL, Jordan SW, Hersam MC, Shah RN. Three-dimensional printing of high-content graphene scaffolds for electronic and biomedical applications. *ACS Nano*. 2015;9(4):4636-4648. doi: 10.1021/acsnano.5b01179
11. Huang H, Zhang B, Zhong J, et al. The behavior between fluid and structure from coupling system of bile, bile duct, and polydioxanone biliary stent: a numerical method. *Med Eng Phys*. 2023;113:103966. doi: 10.1016/J.MEDENGPHY.2023.103966
12. Xu Y, Zhang F, Zhai W, Cheng S, Li J, Wang Y. Unraveling of advances in 3D-printed polymer-based bone scaffolds. *Polymers*. 2022;14(3). doi: 10.3390/polym14030566
13. Valashani SMM, Barrett CJ, Barthelat F. Self-assembly of microscopic tablets within polymeric thin films: a possible pathway towards new hybrid materials. *RSC Adv*. 2015;5(7):4780-4787. doi: 10.1039/c4ra15166f
14. Turnbull G, Clarke J, Picard F, et al. 3D bioactive composite scaffolds for bone tissue engineering. *Bioact Mater*. 2018;3(3):278-314. doi: 10.1016/j.bioactmat.2017.10.001

15. Szojka A, Lalh K, Andrews SHJ, Jomha NM, Osswald M, Adesida AB. Biomimetic 3D printed scaffolds for meniscus tissue engineering. *Bioprinting*. 2017;8:1-7. doi: 10.1016/j.bprint.2017.08.001

16. Kabirian F, Ditkowski B, Zamanian A, Heying R, Mozafari M. An innovative approach towards 3D-printed scaffolds for the next generation of tissue-engineered vascular grafts. *Mater Today Proc*. 2018;5(7):15586-15594. doi: 10.1016/j.matpr.2018.04.167

17. DeStefano V, Khan S, Tabada A. Applications of PLA in modern medicine. *Eng Regen*. 2020;1:76-87. doi: 10.1016/j.engreg.2020.08.002

18. Mota C, Puppi D, Chiellini F, Chiellini E. Additive manufacturing techniques for the production of tissue engineering constructs. *J Tissue Eng Regen Med*. 2015;9(3):174-190. doi: 10.1002/term.1635

19. Chung JJ, Im H, Kim SH, Park JW, Jung Y. Toward biomimetic scaffolds for tissue engineering: 3D printing techniques in regenerative medicine. *Front Bioeng Biotechnol*. 2020;8. doi: 10.3389/fbioe.2020.586406

20. Alagoz AS, Hasirci V. 3D printing of polymeric tissue engineering scaffolds using open-source fused deposition modeling. *Emergent Mater*. 2020;3(4):429-439. doi: 10.1007/s42247-019-00048-2

21. Gillispie G, Prim P, Copus J, et al. Assessment methodologies for extrusion-based bioink printability. *Biofabrication*. 2020;12(2). doi: 10.1088/1758-5090/ab6f0d

22. Papaioannou TG, Manolesou D, Dimakakos E, Tsoucalas G, Vavuranakis M, Tousoulis D. 3D bioprinting methods and techniques: applications on artificial blood vessel fabrication. *Acta Cardiol Sin*. 2019;35(3):284-289. doi: 10.6515/ACS.201905_35(3).20181115A

23. Lee JS, Hong JM, Jung JW, Shim JH, Oh JH, Cho DW. 3D printing of composite tissue with complex shape applied to ear regeneration. *Biofabrication*. 2014;6(2). doi: 10.1088/1758-5082/6/2/024103

24. Lee A, Hudson AR, Shiwarski DJ, et al. 3D bioprinting of collagen to rebuild components of the human heart. *Science*. 2019;365(6452):482-487. doi: 10.1126/science.aav9051

25. Jung JW, Lee JS, Cho DW. Computer-aided multiple-head 3D printing system for printing of heterogeneous organ/tissue constructs. *Sci Rep*. 2016;6. doi: 10.1038/srep21685

26. Liu J, Zhou Y, Lu J, et al. Injectable, tough and adhesive zwitterionic hydrogels for 3D-printed wearable strain sensors. *Chem Eng J*. 2023;475:146340. doi: 10.1016/J.CEJ.2023.146340

27. Ramesh S, Harrysson OLA, Rao PK, et al. Extrusion bioprinting: recent progress, challenges, and future opportunities. *Bioprinting*. 2021;21. doi: 10.1016/j.bprint.2020.e00116

28. Ng WL, Huang X, Shkolnikov V, Suntornnond R, Yeong WY. Polyvinylpyrrolidone-based bioink: influence of bioink properties on printing performance and cell proliferation during inkjet-based bioprinting. *Bio-Des Manuf*. 2023;6(6):676-690. doi: 10.1007/s42242-023-00245-3

29. Chartrain NA, Williams CB, Whittington AR. A review on fabricating tissue scaffolds using vat photopolymerization. *Acta Biomater*. 2018;74:90-111. doi: 10.1016/j.actbio.2018.05.010

30. Moroni L, Boland T, Burdick JA, et al. Biofabrication: a guide to technology and terminology. *Trends Biotechnol*. 2018;36(4):384-402. doi: 10.1016/j.tibtech.2017.10.015

31. Mwema FM, Akinlabi ET. Basics of fused deposition modelling (FDM). In: Castro M, eds. *SpringerBriefs in Applied Sciences and Technology*. Cham, Switzerland: Springer; 2020: 1-15. doi: 10.1007/978-3-030-48259-6_1

32. Hoque ME, Chuan YL, Pashby I. Extrusion based rapid prototyping technique: an advanced platform for tissue engineering scaffold fabrication. *Biopolymers*. 2012;97(2):83-93. doi: 10.1002/bip.21701

33. Gross BC, Erkal JL, Lockwood SY, Chen C, Spence DM. Evaluation of 3D printing and its potential impact on biotechnology and the chemical sciences. *Anal Chem*. 2014;86(7):3240-3253. doi: 10.1021/ac403397r

34. Yazar A, Top N, Bülbül R, Şahin I. Effect of infill density and infill pattern on mechanical properties in fused deposition modeling (FDM). In: *Proceedings of the Innovative Approaches in Additive Manufacturing Congress (IA4AM). Gazi University;* 2021.

35. Fernandez-Vicente M, Calle W, Ferrandiz S, Conejero A. Effect of infill parameters on tensile mechanical behavior in desktop 3D printing. *3D Print Addit Manuf*. 2016;3(3):183-192. doi: 10.1089/3dp.2015.0036

36. Zein I, Hutmacher DW, Cheng Tan K, Hin Teoh S. Fused deposition modeling of novel scaffold architectures for tissue engineering applications. *Biomaterials*. 2002;23(4):1169-1185. doi: 10.1016/S0142-9612(01)00232-0

37. Boparai KS, Singh R, Singh H. Development of rapid tooling using fused deposition modeling: a review. *Rapid Prototyp J*. 2016;22(2):281-299. doi: 10.1108/RPJ-04-2014-0048

38. Günaydın K, Türkmen HS. Common FDM 3D printing defects. In: *Proceedings of the International Congress on 3D Printing (Additive Manufacturing) Technologies and Digital Industry*; 2018.

39. Gupta S, Bissoyi A, Bit A. A review on 3D printable techniques for tissue engineering. *Bionanoscience*. 2018;8(3):868-883. doi: 10.1007/s12668-018-0525-4

40. Yang S, Leong KF, Du ZME, Chua CK. The design of scaffolds for use in tissue engineering. Part II. Rapid prototyping techniques. *Tissue Eng*. 2002;8(1):1-11. doi: 10.1089/107632702753503009

41. Sukindar NA, Ariffin MKA, Baharudin BTHT, Jaafar CNA, Ismail MIS. Analyzing the effect of nozzle diameter in fused deposition modeling for extruding polylactic acid using open source 3D printing. *J Teknol*. 2016;78(10):7-15. doi: 10.11113/jt.v78.6265

42. del Barrio Cortés E, Matutano Molina C, Rodríguez-Lorenzo L, Cubo-Mateo N. Generation of controlled micrometric fibers inside printed scaffolds using standard FDM 3D printers. *Polymers*. 2023;15(1). doi: 10.3390/polym15010096

43. Zhang Y, Harrison C. Tomo: wearable, low-cost, electrical impedance tomography for hand gesture recognition. In: *Proceedings of the 28th Annual ACM Symposium on User Interface Software and Technology*. Association for Computing Machinery, Inc.; 2015:167-173. doi: 10.1145/2642918.2647356

44. Lu Q, Song KY, Feng Y, Xie J. Fabrication of suspended uniform polymer microfibers by FDM 3D printing. *CIRP J Manuf Sci Technol*. 2021;32:179-187. doi: 10.1016/j.cirpj.2020.11.005

45. Paraskevoudis K, Karayannis P, Koumoulos EP. Real-time 3d printing remote defect detection (Stringing) with computer vision and artificial intelligence. *Processes*. 2020;8(11):1-15. doi: 10.3390/pr8111464

46. Visscher DO, Bos EJ, Peeters M, et al. Cartilage tissue engineering: preventing tissue scaffold contraction using a 3D-printed polymeric cage. *Tissue Eng Part C Methods*. 2016;22(6):573-584. doi: 10.1089/ten.tec.2016.0073

47. Zhang Z, He H, Fu W, Ji D, Ramakrishna S. Electro-hydrodynamic direct-writing technology toward patterned ultra-thin fibers: advances, materials and applications. *Nano Today*. 2020;35. doi: 10.1016/j.nantod.2020.100942

48. Lannutti J, Reneker D, Ma T, Tomasko D, Farson D. Electrospinning for tissue engineering scaffolds. *Mater Sci Eng C*. 2007;27(3):504-509. doi: 10.1016/j.msec.2006.05.019

49. Chlanda A, Kijeńska E, Święszkowski W. Microscopic methods for characterization of selected surface properties of biodegradable, nanofibrous tissue engineering scaffolds. In: *Proceedings of the Materials Science Forum*. Trans Tech Publications Ltd; 2017:213-216. doi: 10.4028/www.scientific.net/MSF.890.213

50. Kara Y, Kovács NK, Nagy-György P, Boros R, Molnár K. A novel method and printhead for 3D printing combined nano-/microfiber solid structures. *Addit Manuf*. 2023;61. doi: 10.1016/j.addma.2022.103315

51. Gleadall A. FullControl GCode designer: open-source software for unconstrained design in additive manufacturing. *Addit Manuf*. 2021;46. doi: 10.1016/j.addma.2021.102109

52. Naghieh S, Badrossamay M, Foroozmehr E, Kharaziha M. Combination of PLA micro-fibers and PCL-gelatin nano-fibers for development of bone tissue engineering scaffolds. *IJSIEC*. 2017;6(1):1-4. doi: 10.4172/2090-4908.1000150

53. Molde J, Steele JAM, Pastino AK, Mahat A, Murthy NS, Kohn J. A step toward engineering thick tissues: distributing microfibers within 3D printed frames. *J Biomed Mater Res A*. 2020;108(3):581-591. doi: 10.1002/jbm.a.36838

54. Corapi D, Morettini G, Pascoletti G, Zitelli C. Characterization of a polylactic acid (PLA) produced by fused deposition modeling (FDM) technology. *Procedia Struct Integr*. 2019;24:289-295. doi: 10.1016/j.prostr.2020.02.026

55. Nagarajan S, Radhakrishnan S, Kalkura SN, Balme S, Miele P, Bechelany M. Overview of protein-based biopolymers for biomedical application. *Macromol Chem Phys*. 2019;220(14). doi: 10.1002/macp.201900126

56. Ebrahimi F, Ramezani Dana H. Poly lactic acid (PLA) polymers: from properties to biomedical applications. *Int J Polym Mater Polym Biomater*. 2022;71(15):1117-1130. doi: 10.1080/00914037.2021.1944140

57. Gregor A, Filová E, Novák M, et al. Designing of PLA scaffolds for bone tissue replacement fabricated by ordinary commercial 3D printer. *J Biol Eng*. 2017;11(1). doi: 10.1186/s13036-017-0074-3

58. Wasyłeczko M, Sikorska W, Chwojnowski A. Review of synthetic and hybrid scaffolds in cartilage tissue engineering. *Membranes*. 2020;10(11):1-28. doi: 10.3390/membranes10110348

59. Szojka A, Lalh K, Andrews SHJ, Jomha NM, Osswald M, Adesida AB. Biomimetic 3D printed scaffolds for meniscus tissue engineering. *Bioprinting*. 2017;8:1-7. doi: 10.1016/j.bprint.2017.08.001

60. Singhvi MS, Zinjarde SS, Gokhale DV. Polylactic acid: synthesis and biomedical applications. *J Appl Microbiol*. 2019;127(6):1612-1626. doi: 10.1111/jam.14290

61. Lasprilla AJR, Martinez GAR, Lunelli BH, Jardini AL, Filho RM. Poly-lactic acid synthesis for application in biomedical devices - a review. *Biotechnol Adv*. 2012;30(1):321-328. doi: 10.1016/j.biotechadv.2011.06.019

62. Alafaghani A, Qattawi A, Ablat MA. Design consideration for additive manufacturing: fused deposition modelling. *Open J Appl Sci*. 2017;7(6):291-318. doi: 10.4236/ojapps.2017.76024

63. Zhang B, Seong B, Nguyen VD, Byun D. 3D printing of high-resolution PLA-based structures by hybrid electrohydrodynamic and fused deposition modeling techniques. *J Micromech Microeng*. 2016;26(2). doi: 10.1088/0960-1317/26/2/025015

64. Heljak MK, Kurzydlowski KJ, Swieszkowski W. Computer aided design of architecture of degradable tissue engineering scaffolds. *Comput Methods Biomech Biomed Engin*. 2017;20(15):1623-1632. doi: 10.1080/10255842.2017.1399263

65. Chen S, McCarthy A, John JV, Su Y, Xie J. Converting 2D nanofiber membranes to 3D hierarchical assemblies with structural and compositional gradients regulates cell behavior. *Adv Mater*. 2020;32(43). doi: 10.1002/adma.202003754

66. Collins MN, Ren G, Young K, Pina S, Reis RL, Oliveira JM. Scaffold fabrication technologies and structure/function properties in bone tissue engineering. *Adv Funct Mater*. 2021;31(21). doi: 10.1002/adfm.202010609

67. Choi WJ, Hwang KS, Kwon HJ, et al. Rapid development of dual porous poly(lactic acid) foam using fused deposition modeling (FDM) 3D printing for medical scaffold application. *Mater Sci Eng C*. 2020;110. doi: 10.1016/j.msec.2020.110693

68. Söhling N, Neijhoft J, Nienhaus V, et al. 3D-printing of hierarchically designed and osteoconductive bone tissue engineering scaffolds. *Materials*. 2020;13(8). doi: 10.3390/MA13081836

69. Sankaravel SG, Syed RB, Manivachakan V. In vitro and mechanical characterization of PLA/egg shell biocomposite scaffold manufactured using fused deposition modeling technology for tissue engineering applications. *Polym Compos*. 2022;43(1):1-638. doi: 10.1002/pc.26365

70. da Silva K, Kumar P, Choonara YE, du Toit LC, Pillay V. Three-dimensional printing of extracellular matrix (ECM)-mimicking scaffolds: a critical review of the current ECM materials. *J Biomed Mater Res A*. 2020;108(12): 2324-2350. doi: 10.1002/jbm.a.36981

71. Zaszczyńska A, Moczulska-Heljak M, Gradys A, Sajkiewicz P. Advances in 3D printing for tissue engineering. *Materials*. 2021;14(12). doi: 10.3390/ma14123149

72. Tamay DG, Usal TD, Alagoz AS, Yucel D, Hasirci N, Hasirci V. 3D and 4D printing of polymers for tissue engineering applications. *Front Bioeng Biotechnol*. 2019;7(JUL). doi: 10.3389/fbioe.2019.00164

73. Gleadall A, Visscher D, Yang J, Thomas D, Segal J. Review of additive manufactured tissue engineering scaffolds: relationship between geometry and performance. *Burns Trauma*. 2018;6. doi: 10.1186/s41038-018-0121-4

74. Baptista R, Guedes M, Pereira MFC, Maurício A, Carrelo H, Cidade T. On the effect of design and fabrication parameters on mechanical performance of 3D printed PLA scaffolds. *Bioprinting*. 2020;20. doi: 10.1016/j.bprint.2020.e00096

75. Schneider M, Fritzsche N, Puciul-Malinowska A, et al. Surface etching of 3D printed poly(lactic acid) with NaOH: a systematic approach. *Polymers*. 2020;12(8). doi: 10.3390/POLYM12081711

76. Guduric V, Metz C, Siadous R, et al. Layer-by-layer bioassembly of cellularized polylactic acid porous membranes for bone tissue engineering. *J Mater Sci Mater Med*. 2017;28(5). doi: 10.1007/s10856-017-5887-6